1 H Pulsed ENDOR and ESEEM Evidence That the Bis-imidazole Complexes of Iron(III) Tetraphenylchlorin and Tetraphenylporphyrin Have the Same Order of g Values, and the Same Electron…

ARTICLE *in* JOURNAL OF THE AMERICAN CHEMICAL SOCIETY · MARCH 2001

Impact Factor: 12.11 · DOI: 10.1021/ja002777y

3 AUTHORS, INCLUDING:

Arnold M Raitsimring
The University of Arizona
123 PUBLICATIONS **2,579** CITATIONS
SEE PROFILE

F(rances) Ann Walker
The University of Arizona
240 PUBLICATIONS **8,648** CITATIONS
SEE PROFILE

^{1}H Pulsed ENDOR and ESEEM Evidence That the Bis-imidazole Complexes of Iron(III) Tetraphenylchlorin and Tetraphenylporphyrin Have the Same Order of *g* Values, and the Same Electronic Ground State

Andrei V. Astashkin,* Arnold M. Raitsimring, and F. Ann Walker

Contribution from the Department of Chemistry, University of Arizona, Tucson, Arizona 85721-0041

Received July 27, 2000

Abstract: The electronic structures of the bis-imidazole complexes of iron(III) tetraphenylporphyrin ([(TPP)Fe(ImH)$_2$]$^+$) and iron(III) tetraphenylchlorin ([(TPC)Fe(ImH)$_2$]$^+$) in frozen glassy solutions have been studied by the pulsed electron nuclear double resonance (ENDOR) technique of Mims and by electron spin−echo envelope modulation (ESEEM) spectroscopy. ESEEM spectra have been used to determine the orientation of the imidazole ligand planes with repect to the **g** tensor axes. In the ENDOR spectra, the manifestations of the implicit TRIPLE effect described and explained earlier by Doan et al. (*J. Am. Chem. Soc.* **1996**, *118*, 7014) were seen. In this work, the explicit expressions describing this effect were derived for the first time and used to successfully simulate the proton ENDOR spectra at the low- (LF) and high-field (HF) edges of the EPR spectrum. Using pulsed ENDOR, we have been able to determine the spin density distributions in the π-systems of both tetrapyrroles and show that [(TPC)Fe(ImH)$_2$]$^+$ has the electronic orbital ground state $(d_{xy})^2(d_{xz},d_{yz})^3$, the same as that known for [(TPP)Fe(ImH)$_2$]$^+$, and the largest principal *g* value corresponds to the **g** tensor axis **3**, which is normal to the heme plane. For the TPP complex, the **g** tensor axis **1**, corresponding to the smallest principal *g* value, was found to be at an angle φ_1 of 30−35° from the N−Fe−N axis, with the ligand planes rotated by the angle of 20−25° in the opposite direction. For the TPC complex, φ_1 was found to be about 25° from the direction N_I−Fe−N_{III}, where N_I corresponds to the nitrogen of the saturated pyrrole ring. The ligand planes in this complex were found to be oriented at an angle of about 10° in the opposite direction.

Introduction

The electronic orbital states of iron porphyrin complexes are often described in terms of the populations of the various d orbitals, d_{xy}, d_{xz}, d_{yz}, d_{z^2}, $d_{x^2-y^2}$, appropriate for the symmetry of such systems. When the immediate ligands to the central iron ion are considered as point charges, the symmetry group is usually D_{2h}, with the symmetry axes **X**, **Y**, and **Z** aligned with the three mutually perpendicular iron−ligand directions defining the molecular coordinate frame. The magnetic axes **1**, **2** and **3** in this approximation coincide with **X**, **Y**, and **Z**, respectively. In this work, following common practice, we orient the molecular frame axes **X** and **Y** along the porphyrin nitrogen directions (N−Fe−N) and take **Z** as normal to the heme plane.

The problem of evaluation of the orbital configuration of the low-spin Fe(III) from the principal *g* values measured in the electron paramagnetic resonance (EPR) experiment has been addressed in numerous publications.[1−12] Using the expressions derived by the authors of these papers, one can readily infer the nature of the ground electronic orbital state of low-spin d^5 centers, that is, whether the unpaired electron is mainly localized in one of the d_π orbitals (d_{yz} or d_{xz}), or instead, in the d_{xy} orbital, in the porphyrin plane. There is, however, a difficulty in applying this knowledge to chemical problems or to interpreting the spectroscopic data obtained from other magnetic techniques (ESEEM, Mössbauer, MCD, NMR).[13] It originates from the fact that, without any additional information, the principal *g* values can be assigned to **1**, **2**, and **3** (or **X**, **Y**, and **Z** in our current approximation) in various ways. Depending on the assignment, either the d_{xy} or d_π ground state can be obtained.

It is the combined use of X-ray crystallography and single-crystal EPR spectroscopy that can assign the principal *g* values to the directions of magnetic axes in the molecular coordinate frame and find the d orbital of the unpaired electron. In this way the problem of the orientation of the magnetic axes with respect to the molecular frame has been solved for several iron(III) porphyrin complexes and ferriheme proteins.[14−20] For orientationally disordered complexes (frozen solution or pow-

* Corresponding author. On leave from the Institute of Chemical Kinetics and Combustion, Russian Academy of Sciences, Novosibirsk 630090, Russia.

(1) Bleaney, B.; O'Brien, M. C. M. *Proc. Phys. Soc. B* **1956**, *69*, 1216.
(2) Griffith, J. S. *Nature* **1957**, *180*, 30.
(3) Kotani, M. *Supp. Prog. Theor. Phys.* **1961**, *17*, 4.
(4) Weissbluth, M. *Struct. Bonding* **1967**, *2*, 1.
(5) Oosterhuis, W. T.; Lang, G. *Phys. Rev.* **1969**, *178*, 439.
(6) Loew, G. M. H. *Biophys. J.* **1970**, *10*, 196.
(7) Griffith, J. S. *Mol. Phys.* **1971**, *21*, 135.
(8) Taylor, C. P. S. *Biochim. Biophys. Acta* **1977**, *491*, 137.
(9) Bohan, T. L. *J. Magn. Reson.* **1977**, *26*, 109.
(10) Rieger, P. H. *Coord. Chem. Rev.* **1994**, *135/136*, 203.
(11) McGarvey, B. R. *Quim. Nova* **1998**, *21*, 206.
(12) McGarvey, B. R. *Coord. Chem. Rev.* **1998**, *170*, 75.
(13) Walker, F. A. *Coord. Chem. Rev.* **1999**, *185/186*, 471.
(14) Hori, H. *Biochim. Biophys. Acta* **1971**, *251*, 227.
(15) Mailer, C.; Taylor, C. P. S. *Can. J. Biochem.* **1972**, *50*, 1048.
(16) Devaney, P. W. Ph.D. Thesis, University of Illinois, 1980.
(17) Byrn, M. P.; Katz, B. A.; Keder, N. L.; Levan, K. R.; Magurany, C. J.; Miller, K. M.; Pritt, J. W.; Strouse, C. E. *J. Am. Chem. Soc.* **1983**, *105*, 4916.
(18) Quinn, R.; Valentine, J. S.; Byrn, M. P.; Strouse, C. E. *J. Am. Chem. Soc.* **1987**, *109*, 3301.
(19) Soltis, S. M.; Strouse, C. E. *J. Am. Chem. Soc.* **1988**, *110*, 2824.

10.1021/ja002777y CCC: $20.00
Published on Web 02/07/2001

dered solids), the same problem can be solved with the aid of high-resolution EPR techniques, using the ligand protons[21−24] and nitrogens[25,26] as reference nuclei.

For the bis-imidazole complex of iron(III) tetraphenylporphyrin ($[(TPP)Fe(ImH)_2]^+$),[18] in particular (as well as for a number of other low-spin ferriheme systems[14−24]), it is well established that the axis of the largest principal *g* value is normal to the heme plane, and thus the unpaired electron occupies the π-bonding d_{yz} orbital. However, to our knowledge, no single-crystal EPR studies have ever been performed for the analogous chlorin system, the bis-imidazole complex of iron(III) tetraphenylchlorin ($[(TPC)Fe(ImH)_2]^+$), and thus the problem of assigning a certain orbital ground state to this complex remains unsolved.

As our long-term goal is to establish correlations between the chemical and electronic structures of various heme complexes, it has become important to determine with certainty the electronic orbital ground state of low-spin Fe(III) chlorins, specifically $[(TPC)Fe(ImH)_2]^+$. In particular, it was desired to determine whether the largest or the smallest *g* value of $[(TPC)Fe(ImH)_2]^+$ corresponds to the direction along the heme plane normal (**Z**), and thus whether the electronic ground state of $[(TPC)Fe(ImH)_2]^+$ is the same as or different from that of the corresponding porphyrin complex, $[(TPP)Fe(ImH)_2]^+$. In this work we apply pulsed electron nuclear double resonance (ENDOR) and electron spin−echo envelope modulation (ESEEM) methods to establish the orientation of the **g** tensor of $[(TPC)Fe(ImH)_2]^+$ with respect to the molecular coordinate frame and to find the orientation of the imidazole ligand planes with respect to the **g** tensor axes **1** and **2**.

Experimental Section

The tetraphenylchlorin free base, $TPCH_2$, was purchased from Porphyrin Products, Provo, UT. Iron was inserted as described previously,[27] with the exception that molecular oxygen was rigorously excluded until workup, because of the ease of reoxidation of the chlorin to the parent porphyrin. Workup consisted only of washing the chloroform solution repeatedly to remove excess iron salts, followed by brief shaking with a solution of saturated aqueous NaCl at pH 2 and drying over anhydrous sodium sulfate. Samples of (TPC)FeCl prepared in this manner routinely showed less than 5% contamination with (TPP)FeCl. The chloroiron(III) tetraphenylporphyrin was prepared as described previously.[27] Solutions of the low-spin Fe(III) tetrapyrrole macrocycles (~5 mM) for EPR and pulsed EPR experiments were prepared in deuterated solvents (Cambridge Isotopes), CD_2Cl_2 in the case of TPP and DMF-d_7 in the case of TPC. Both protonated and deuterated imidazole, Im-h_4 and Im-d_4, respectively, were purchased from Aldrich. Approximately four equivalents of imidazole per equivalent of iron(III) tetrapyrrole macrocycle were added to ensure complete formation of the bis-imidazole complex in each case.

The pulsed ENDOR experiments were carried out on the home-built X/P-band pulsed EPR spectrometer,[28] which was recently upgraded to implement more flexible secondary timing, and equipped with a pulsed ENDOR accessory. The ENDOR cavity has been described elsewhere.[29] The output power of the radio frequency (RF) amplifier was about 200 W. The microwave (mw) carrier frequency ν_{mw} in these experiments was about 15 GHz (P-band), and the pulsed ENDOR technique developed by Mims[30] was employed.

The purpose of the ENDOR experiments was to determine the orientation of the *g* frame with respect to the porphyrin or chlorin plane, using the porphyrin/chlorin protons as reference nuclei. Therefore, for these experiments, the imidazole ligands, as well as the solvents, were completely deuterated. On the other hand, for the ESEEM experiments, determination of the orientation of the imidazole ligands with respect to the **g** tensor was the goal. Therefore, in the ESEEM experiments the protonated imidazole was used. The ESEEM measurements at the high-field turning points of the EPR spectra were performed on the S/C band pulsed EPR spectrometer.[31] The measurement temperature was about 4.2 K.

Mims ENDOR Theory

The Mims ENDOR technique[30] is based on the three-pulse stimulated ESE sequence. The first two mw pulses are separated by the time interval τ. The second and third mw pulses are separated by the time interval *T*. During this interval the RF pulse is applied. We will consider the nominal flip angle for this pulse to be 180°, which nearly maximizes the ENDOR effect.

According to simple theory,[32,33] when the RF pulse is in resonance with a nuclear transition at one of the electron spin manifolds, the amplitude of the stimulated ESE signal due to the electrons coupled to that nucleus is

$$V_{RF}(\tau) = \frac{1}{2}[1 + \cos(2\pi A\tau)] \quad (1)$$

where *A* is the secular component of the hyperfine interaction (hfi). In the absence of resonant RF, the amplitude of the ESE signal is $V_{NoRF}(\tau) = 1$, and thus the ENDOR effect is:

$$\Delta V(\tau) = V_{NoRF}(\tau) - V_{RF}(\tau) = \frac{1}{2}[1 - \cos(2\pi A\tau)] \quad (2)$$

It follows from eq 2 that the maxima of the ENDOR effect correspond to the hfi values $A = \pm[\nu + 1/2]/\tau$ (where $\nu \geq 0$ is an integer number), while the hfi values $A = \pm\nu/\tau$ lead to $\Delta V = 0$, producing a series of "blind spots" in the Mims ENDOR spectrum.

To a first approximation, the transition frequencies of weakly (compared to the Zeeman interaction) coupled nuclei with zero quadrupole interaction (e.g., protons) are given by

$$\nu_\alpha = \nu_I - A/2; \quad \nu_\beta = \nu_I + A/2 \quad (3)$$

where the subscripts α and β denote the electron spin manifolds and ν_I is the nuclear Zeeman frequency. The hfi constant *A* is expressed as

(20) Inniss, D.; Soltis, S. M.; Strouse, C. E. *J. Am. Chem. Soc.* **1998**, *110*, 5644.
(21) Raitsimring, A. M.; Borbat, P.; Shokhireva, T. Kh.; Walker, F. A. *J. Phys. Chem.* **1996**, *100*, 5235.
(22) Raitsimring, A. M.; Walker, F. A. *J. Am. Chem. Soc.* **1998**, *120*, 991.
(23) Schhnemann, V.; Raitsimring, A. M.; Benda, R.; Trautwein, A. X.; Shokhireva, T. Kh.; Walker, F. A. *J. Biol. Inorg. Chem.* **1999**, *4*, 708.
(24) Astashkin, A. V.; Raitsimring, A. M.; Walker, F. A. *Chem. Phys. Lett.* **1999**, *306*, 9.
(25) Magliozzo, R. S.; Peisach, J. *Biochemistry* **1992**, *31*, 189.
(26) Lee, H.-I.; Dexter, A. F.; Fann, Y.-C.; Lakner, F. J.; Hager, L. P.; Hoffman, B. M. *J. Am. Chem. Soc.* **1997**, *119*, 4059.
(27) Simonis, U.; Walker, F. A.; Lee, P. L.; Hanquet, B. J.; Meyerhoff, D. J.; Scheidt, W. R. *J. Am. Chem. Soc.* **1987**, *109*, 2659.
(28) Borbat, P. P.; Raitsimring, A. M. *Abstracts of 36th Rocky Mountain Conference on Analytical Chemistry*; Denver, CO, July 3 −August 5, 1994; p 94.
(29) Astashkin, A. V.; Mader Cosper, M.; Raitsimring, A. M.; Enemark, J. H. *Inorg. Chem.* **2000**, *39*, 4989.
(30) Mims, W. B. *Proc. R. Soc. London* **1965**, *283*, 482.
(31) Astashkin, A. V.; Kozlyuk, V.; Raitsimring, A. M. *Abstracts of 40th Rocky Mountain Conference on Analytical Chemistry*; Denver, CO, July 26−30, 1998; additional materials.
(32) Grupp, A.; Mehring, M. In *Modern Pulsed and Continuous Wave Electron Spin Resonance*; Kevan, L., Bowman, M., Eds.; Wiley: New York, 1990; p 195.
(33) Thomann, H.; Bernardo, M. In *Methods in Enzymology*; Riordan, J. F., Vallee, B. L., Eds.; Academic Press: San Diego, 1993; Vol. 227, p 118.

$$A = a_{iso} + T_{sec} \quad (4)$$

where a_{iso} is the isotropic hfi constant and T_{sec} is the secular part of the anisotropic hfi. Taken together, eqs 2 and 3 predict the ENDOR spectrum consisting of pairs of lines of equal intensity, situated symmetrically with respect to the nuclear Zeeman frequency ν_I.

Such a perfect symmetry of the ENDOR spectrum with respect to ν_I can be disrupted by the nonsecular components of the anisotropic hfi, by different Rabi frequencies of the nuclear spins coupled to different electron spin manifolds,[32,33] and by the frequency dependence of the RF field intensity. However, usually, within the frequency range of a narrow ENDOR spectrum, these intensity distortions are very insignificant.

A recent refinement to this simple theory due to Doan et al.[34] takes into account the effect of simultaneous interaction of the electron spin with several nuclei. Some of these nuclei contribute to the ENDOR spectrum, while the others, so-called reference nuclei, may be out of the ENDOR range. The prediction of their theory is that the ENDOR effect will be affected by the ESEEM from the reference nuclei. We wish now to reformulate the result of that work[34] in explicit form, using the density matrix formalism.[35]

Let us select one nucleus observed by ENDOR and consider it separately from all other (reference) nuclei. The time interval T is assumed to be sufficiently long to ensure the complete damping of the nuclear coherences by the time when the third mw pulse is applied. It is easy to show that the dependence of the stimulated ESE amplitude on τ is described by the expression:

$$V(\tau) \propto \frac{1}{2}\left[V_N^{\alpha}(\tau)V_R^{\alpha}(\tau) + V_N^{\beta}(\tau)V_R^{\beta}(\tau)\right] \quad (5)$$

where V_N and V_R are the contributions to the stimulated ESEEM from the nucleus observed by ENDOR and from the reference nuclei, respectively. The superscripts α and β denote the electron spin manifolds. Without RF, eq 5 describes the usual product rule for the stimulated ESEEM in the case of an unpaired electron interacting with several nuclei.[36] The density matrix analysis shows that this rule holds also for the case of the resonant RF irradiation, which is readily understandable because the RF swaps only the nuclear spin manifolds, but not the electronic ones.

If the RF pulse is in resonance with the transition of the nucleus at the α (β) electron spin manifold, the ENDOR effect can be written as

$$\Delta V(\tau) \propto \frac{1}{2}\Delta V_N^{\alpha(\beta)}(\tau)V_R^{\alpha(\beta)}(\tau) \quad (6)$$

where $\Delta V_N^{\alpha(\beta)}$ is the difference between the values of $V_N^{\alpha(\beta)}$ without and with RF.

Without RF, for the monitored nucleus with $I = {}^1/_2$ (e.g., proton), V_N^{α} and V_N^{β} are:[36]

$$\Delta V_N^{\alpha(\beta)}(\tau) = 1 - \frac{k}{2}(1 - \cos\omega_{\beta(\alpha)}\tau) \quad (7)$$

where $\omega_{\alpha(\beta)} = 2\pi\nu_{\alpha(\beta)}$ and k is the usual modulation amplitude factor.[36]

If the RF pulse inverts the nuclear spin projections at the α (β) electron spin manifolds, $V_N^{\alpha(\beta)}$ can be obtained in a straightforward manner:

$$V_N^{\alpha(\beta)}(\tau) = \left[\frac{1+\sqrt{1-k}}{2}\right]^2 \cos\omega_{\delta}\tau + \left[\frac{1-\sqrt{1-k}}{2}\right]^2 \cos\omega_{\sigma}\tau + \frac{k}{2}\cos\omega_{\alpha(\beta)}\tau \quad (8)$$

where $\omega_{\delta} = \omega_{\alpha} - \omega_{\beta}$ and $\omega_{\sigma} = \omega_{\alpha} + \omega_{\beta}$. Equations 7 and 8 immediately lead to

$$\Delta V_N^{\alpha(\beta)}(\tau) = \left[\frac{1+\sqrt{1-k}}{2}\right]^2 [1 - \cos\omega_{\delta}\tau] + \left[\frac{1-\sqrt{1-k}}{2}\right]^2 [1 - \cos\omega_{\sigma}\tau] + \frac{k}{2}[\cos\omega_{\beta(\alpha)}\tau - \cos\omega_{\alpha(\beta)}\tau] \quad (9)$$

For weakly coupled protons, especially if the experiment is performed at high magnetic fields, we have $k \cong 0$ and $\omega_{\delta} \cong 2\pi A$. Equation 9 then reduces to

$$\Delta V_N^{\alpha(\beta)}(\tau) = [1 - \cos 2\pi A\tau] \quad (10)$$

and the total ENDOR effect is

$$\Delta V(\tau) \propto \frac{1}{2}(1 - \cos 2\pi A\tau)V_R^{\alpha(\beta)}(\tau) \quad (11)$$

which, in the absence of ESEEM from the reference nuclei ($V_R^{\alpha(\beta)}(\tau) = 1$) reduces to eq 2.

In the situation of deep ESEEM $V_R^{\alpha(\beta)}$, depending on τ, two limiting cases may be encountered. It may happen that at a given τ $V_R^{\alpha} \cong V_R^{\beta}$, which leads to a symmetric ENDOR spectrum. The other limiting case is that of $V_R^{\alpha(\beta)} \cong 0$, $V_R^{\beta(\alpha)} \neq 0$, which results in a highly asymmetric ENDOR spectrum showing only the transitions that belong to the β (α) electron spin manifold. Of course, any situation falling between these limits is conceivable.

In the original work[34] the dependence of the ENDOR spectrum on the ESEEM produced by the reference nuclei was called an implicit TRIPLE effect because it correlates the transitions of nuclei observed by ENDOR with the transitions of the reference nuclei accomplished by reorientations of the electron spin by the mw pulses. This effect should not be confused with the "ESEEM edited ENDOR" that simply reflects the changes in the relative contributions of two (or more) paramagnetic centers with overlapping EPR spectra to the ENDOR spectrum, if at least one of these paramagnetic centers shows a strong ESEEM.[33]

For oriented paramagnetic centers, the implicit TRIPLE effect does not complicate the analysis of the ENDOR spectra. These spectra may be easily simulated if an additional parameter, a relative statistical weight of the electron spin manifold $W_{\alpha(\beta)}$ is introduced. If $W_{\alpha} \cong W_{\beta} \cong {}^1/_2$ or $W_{\alpha(\beta)} \cong 0$, $W_{\beta(\alpha)} \cong 1$, we have one of the limiting cases described above. The oriented situation takes place at the low- and high-field turning points of the EPR spectrum of ferriheme centers (and other species with essentially rhombic g factor). However, for an orientationally disordered situation, when the ESEEM frequencies and amplitudes of the reference nuclei strongly depend on the orientation, simulation of the ENDOR spectrum may prove impossible without the simultaneous simulation of the ESEEM due to the reference nuclei. Such a situation will be encountered for the intermediate turning point of the EPR spectrum of ferrihemes, and therefore

(34) Doan, P. E.; Nelson, M. J.; Jin, H.; Hoffman, B. M. *J. Am. Chem. Soc.* **1996**, *118*, 7014.
(35) Mims, W. B. *Phys. Rev. B* **1972**, *5*, 2409.
(36) Dikanov, S. A.; Tsvetkov, Yu. D. *Electron Spin−Echo Envelope Modulation (ESEEM) Spectroscopy*; CRC Press: Boca Raton, FL, 1992.

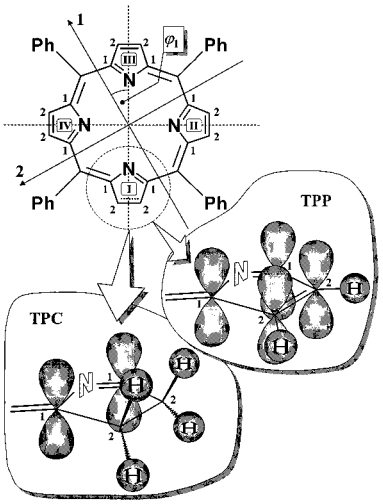

Figure 1. Generic structure of the tetrapyrrole macrocycles TPP and TPC with the numbering of the carbon atoms as used in the discussion of the ENDOR results. **1** and **2** are two of the principal axes of the **g** tensor. The third axis, **3**, is normal to the heme plane. In the lower part of the figure are shown 3D sketches of ring I for TPP and TPC.

we have not performed the ENDOR simulations for this turning point of the EPR spectrum in this work.

Results and Discussion

Figure 1 shows the structure of the iron(III) complexes of the TPP and TPC tetrapyrroles, which only differ in the state of saturation of the outer carbons in pyrrole ring I. Three-dimensional sketches of this ring are shown in the same figure. **1** and **2** are the principal axes of the **g** tensor within the macrocycle plane. We allow these axes to rotate away from the lines joining the opposing pyrrole nitrogens by the angle φ_1 to account for the contribution of the arbitrarily oriented imidazole ligands to the in-plane crystal field components. The orientation of these ligands is described by the angle φ_{lig} between the N_I-Fe-N_{III} axis and the ligand planes. The positive angles φ_1 and φ_{lig} correspond to a rotation in the counterclockwise direction.

Axis **3** of the **g** tensor is normal to the heme plane. Complete numbering of all atoms is not included in Figure 1. Instead, we have numbered only the carbons essential for our discussion of the ENDOR spectra below. The carbons in the pyrrole rings adjacent to the nitrogen atoms are collectively denoted by number 1. The outer carbons in the pyrrole rings are denoted by number 2.

The pulsed ENDOR experiments have been performed at magnetic fields corresponding to the canonical orientations of the **g** tensor with respect to the direction of magnetic field $\mathbf{B_o}$. The various spectroscopic values referring to the low-, intermediate-, and high-field turning points of the EPR spectra will hereafter be denoted by the "LF", "IF", and "HF" subscripts, respectively. The principal *g* values for the TPP complex, written using this notation, are $|g_{HF}| \approx 1.55$, $|g_{IF}| \approx 2.30$, and $|g_{LF}| \approx 2.92$, and those for the TPC complex are $|g_{HF}| \approx 1.75$, $|g_{IF}| \approx 2.39$, and $|g_{LF}| \approx 2.49$.

For $[(TPP)Fe(Im\text{-}d_4)_2]^+$, g_{LF}, g_{IF}, and g_{HF} correspond to the principal **g** tensor axes **3**, **2**, and **1**, respectively.[18] The situation with TPC is less clear, and it is the purpose of this work to establish the correspondence of the **g** tensor axes to the turning points of the EPR spectrum. Specifically, the assignment of g_{HF} to **1** or **3** is to be made. We accomplish this below using the angular dependence of the anisotropic hfi of protons in the tetrapyrrole macrocycle and axial ligands.

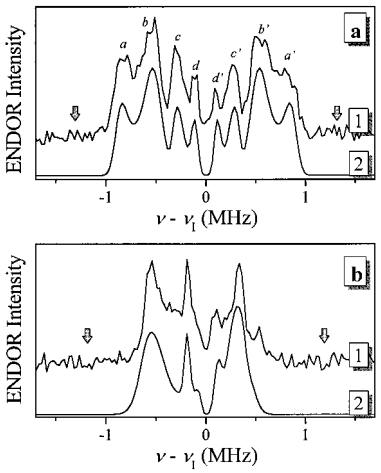

Figure 2. Traces 1 in panels (a) and (b) are Mims ENDOR spectra of $[(TPP)Fe(Im\text{-}d_4)_2]^+$ at g_{LF} ($\mathbf{B_o} = 362$ mT) and g_{HF} ($\mathbf{B_o} = 678$ mT), respectively. Time intervals: (a) $\tau = 380$ ns, $T = 33$ μs, RF pulse duration $t_{RF} = 25$ ms; (b) $\tau = 420$ ns, $T = 33$ μs, $t_{RF} = 25$ μs. Data accumulation time, 1 h for (a) and 6 h for (b). Arrows indicate the blind spots. Traces 2 in both panels are simulations (see text for the hfi parameters).

Traces 1 in Figure 2, a and b, show the pulsed ENDOR spectra of $[(TPP)Fe(Im\text{-}d_4)]^+$ at g_{LF} and g_{HF}, respectively. The spectrum at g_{IF} is not shown because we did not attempt to simulate it for the reasons discussed in the Mims ENDOR Theory section. The spectrum at g_{LF} is practically identical to the CW ENDOR spectrum reported by Scholes et al.[37] (Figure 6 in ref 37). In the latter work, using H→D isotopic substitution, the four inner lines (*c*, *c*′, *d*, and *d*′ in Figure 2a) in the ENDOR spectrum were assigned to the phenyl groups. The inner pair of lines (*dd*′) with 0.2 MHz splitting is due to the *meta* and *para* phenyl protons, and the second pair (*cc*′), with 0.575 MHz splitting, belongs to the *ortho* phenyl protons.[37] The two outer pairs of lines, with splittings of about 1.08 MHz (*bb*′) and 1.68 MHz (*aa*′), are due to the pyrrole protons.[37]

The spectra of $[(TPC)Fe(Im\text{-}d_4)_2]^+$ at g_{LF} and g_{HF} are shown by traces 1 in Figure 3, a and b, respectively. The spectrum at g_{LF} occupies the same range as the corresponding spectrum of the TPP complex (Figure 2), while the spectrum at g_{HF} is considerably broader and exhibits broad features with splittings of about 1.8 and 3.7 MHz. Figure 4 shows the spectra of $[(TPC)Fe(Im\text{-}d_4)_2]^+$ at g_{HF} obtained at different τ values. It follows from these spectra that the features with 1.8 and 3.7 MHz splittings actually represent the wings of very broad lines, the centers of which in Figure 3b are suppressed by the blind spots (shown by arrows).

As follows from the theory of Mims ENDOR outlined above, the implicit TRIPLE effect caused by a deep ESEEM due to ^{14}N nuclei abundant in the iron porphyrins/chlorins may disrupt the symmetry of the ENDOR spectra detected at some or all τ values. The ENDOR spectra of $[(TPC)Fe(Im\text{-}d_4)_2]^+$ at g_{IF} obtained at two different τ values (see Figure 5) demonstrate this effect for the systems studied here. Even greater distortions are seen in Figure 2b, which shows the spectrum of the TPP complex at g_{HF}. The distortions here are so strong that, virtually, the proton transitions within only one electron spin manifold are seen. On the other hand, the spectra of the TPP complex at g_{LF} and of the TPC complex at g_{LF} and g_{HF} shown in Figures 2, 3, and 4 are much more symmetric.

(37) Scholes, C. P.; Falkowski, K. M.; Chen, S.; Bank, J. *J. Am. Chem. Soc.* **1986**, *108*, 1660.

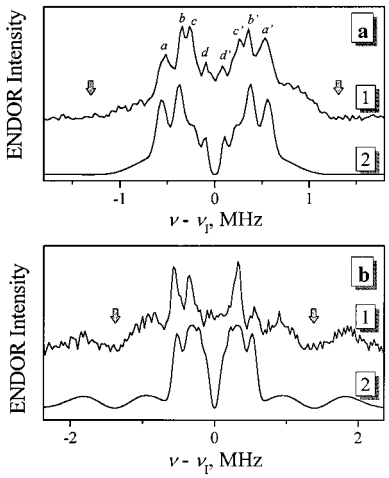

Figure 3. Traces 1 in panels (a) and (b) are Mims ENDOR spectra of [(TPC)Fe(Im-d_4)$_2$]$^+$ recorded at g_{LF} ($\mathbf{B_o} = 432$ mT) and g_{HF} ($\mathbf{B_o} = 596$ mT), respectively. Time intervals: (a) $\tau = 380$ ns, $T = 33$ μs, $t_{RF} = 25$ μs; (b) $\tau = 360$ ns, $T = 33$ μs, $t_{RF} = 25$ μs. Data accumulation time, 2 h for (a) and 7 h for (b). Arrows indicate the blind spots. Traces 2 in both panels are simulations (see text for the hfi parameters).

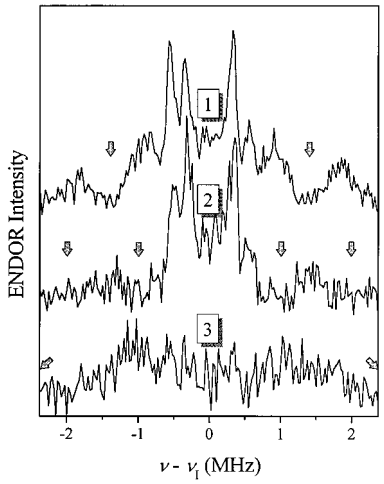

Figure 4. Traces 1, 2, and 3: Mims ENDOR spectra of [(TPC)Fe(Im-d_4)$_2$]$^+$ recorded at g_{HF} ($\mathbf{B_o} = 596$ mT; $T = 33$ μs, $t_{RF} = 25$ μs), at $\tau = 360$, 500, and 200 ns, respectively. Data accumulation time, 7 h, 0.5 h and 0.5 h for traces 1, 2 and 3, respectively. Arrows indicate the blind spots.

Pulsed ENDOR Simulations. In the ENDOR simulations, the positions of the porphyrin (chlorin) protons have been calculated, assuming the heme to be planar and using standard bond lengths. The phenyl ring planes were taken perpendicular to the heme plane, with each phenyl ring situated symmetrically with respect to the heme plane.

The spin density delocalization from the central Fe^{3+} ion to the heme π-system leads to noticeable isotropic hfi constants for some of the heme protons. If the spin density on the carbons in the vicinity of a given proton is large enough, it will also significantly contribute to the anisotropic hfi of this proton. It is necessary to take the latter effect into account, and a simple, though rather crude, model employed in our calculations is now outlined.

There are three distinct types of protons in the systems studied here. The simplest are the phenyl protons, for which $a_{iso} \cong 0$. This is both because the phenyl planes are at rather large angles to the heme plane, thus precluding efficient overlap of the π-systems, and because, at least for the TPP complex, spin delocalization is to the porphyrin 3e(π) orbitals, which have

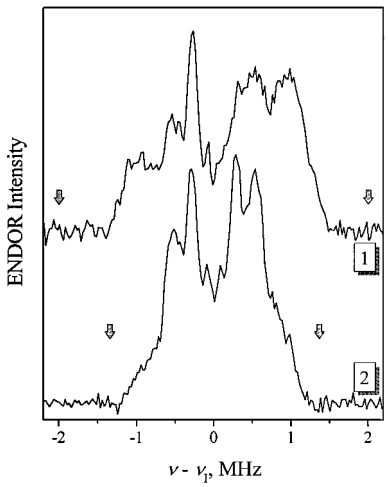

Figure 5. Traces 1 and 2: Mims ENDOR spectra of [(TPC)Fe(Im-d_4)$_2$]$^+$ recorded at g_{IF} ($\mathbf{B_o} = 452$ mT; $T = 33$ μs, $t_{RF} = 25$ μs), at $\tau =$ 250 ns and 370 ns, respectively. Data accumulation time, 1 h for both traces. Arrows indicate the blind spots.

essentially zero amplitude at the *meso* carbons.[38] The anisotropic hfi for the phenyl protons may be approximately calculated under the assumption that the whole spin density is localized on the central Fe^{3+} ion:

$$T_\perp = -\rho_{Fe} g g_n \beta \beta_n / h R_{FeH}^3 \qquad (12)$$

where g and g_n are, respectively, the electronic and nuclear g factors. β and β_n are the Bohr magneton and the nuclear magneton, h is Planck's constant, $\rho_{Fe} \approx 1$ is the spin density on the central Fe atom, and R_{FeH} is the distance between Fe and the proton.

The protons attached to the aromatic pyrrole rings are in the α position with respect to the carbons $C_{(2)}$ (see Figure 1) and are therefore referred to as α protons. Their isotropic hfi constant is determined by the McConnell relation:

$$a_\alpha = Q_\alpha \rho_{C2} \qquad (13)$$

where ρ_{C2} is the spin density on $C_{(2)}$ and $Q_\alpha \cong -63$ MHz.[39]

The anisotropic hfi is treated as a sum of the contributions from the spin densities localized on the central Fe^{3+} ion (as given in eq 12) and on the nearest carbon atom $C_{(2)}$. At $g = 2$, the α proton anisotropic hfi tensor due to ρ_{C2} can be written approximately as ($-30\rho_{C2}$, $30\rho_{C2}$, 0) MHz (see, e.g., ref 40). Thus, for arbitrary g we have ($-15g\rho_{C2}$, $15g\rho_{C2}$, 0) MHz. Since the direction of the Fe$\cdots$H radius-vector, $\mathbf{R_{FeH}}$, is only about 20° away from that of the $C_{(2)}$H bond, the hfi tensors due to ρ_{C2} and ρ_{Fe} are approximately coaxial, and the total anisotropic hfi tensor is

$$T_n \approx -\rho_{Fe} g g_n \beta \beta_n / h R_{FeH}^3; \quad T_{t\perp} \approx T_n - 15g\rho_{C2}; \quad T_{t\parallel} \approx -2T_n + 15g\rho_{C2} \qquad (14)$$

where T_n corresponds to the heme normal, and $T_{t\perp}$ and $T_{t\parallel}$ correspond to the in-plane directions being, respectively,

(38) Walker, F. A. In *The Porphyrin Handbook*; Kadish, K. M., Smith, K. M., Guilard, R., Eds.; Academic Press: San Diego, CA, 2000; Vol. 5, Chapter 36, pp 81−183 and references therein.

(39) McConnell, H. M.; Dearman, H. H. *J. Chem. Phys.* **1958**, *28*, 51.

(40) McConnell, H. M.; Heller, C.; Cole, T.; Fessenden, R. W. *J. Am. Chem. Soc.* **1960**, *82*, 766.

perpendicular and parallel to $\mathbf{R_{FeH}}$. All T values are in MHz. R_{FeH} is about 5.1 Å, which gives T_n about −0.6 MHz for $g = 2$.

The contributions of more distant atoms to the anisotropic hfi are neglected because of considerably greater distances from these atoms to the proton. In addition, the effect of the spin densities delocalized into the heme π-system (apart from that due to the closest carbon) is largely accounted for by using $\rho_{Fe} = 1$ in the calculation.

In the pyrroline ring I of $[(TPC)Fe(Im\text{-}d_4)_2]^+$, the carbons $C_{(2)}$ are approximately sp^3-hybridized. The two protons attached to $C_{(2)}$ are in the β-position with respect to the carbon $C_{(1)}$ participating in the π-system. The isotropic hfi for the β protons (H_β) can be approximated as:

$$a_\beta = Q_\beta \rho_{C1} \cos^2 q \qquad (15)$$

where $Q_\beta \approx 160$ MHz,[41] $\theta \approx 30°$ is the dihedral angle between the $C_{(1)}C_{(2)}H_\beta$ plane and the plane formed by the $C_{(1)}C_{(2)}$ bond and the p orbital on $C_{(1)}$, and ρ_{C1} is the spin density on $C_{(1)}$.

The anisotropic hfi of these protons is mostly due to ρ_{Fe} (eq 12) and ρ_{C1}. The latter contribution is considerably less rhombic than in the case of the α protons, and may be approximated by a formula similar to eq 12, where ρ_{C1} should be substituted for ρ_{Fe}, and the distance $R_{CH} \approx 2.1$ Å between $C_{(1)}$ and H_β should be used instead of R_{FeH}. The corresponding anisotropic hfi tensors are nearly coaxial, and for the total tensor we have

$$T_{\beta\perp} \approx k(\rho_{C1})\cdot\rho_{Fe} g g_n \beta\beta_n / hR^3_{FeH} \qquad (16)$$

where $k(\rho_{C1}) = 1 + \rho_{C1}\cdot(R_{FeH}/R_{CH})^3$. For $R_{FeH} \approx 5$ Å and $R_{CH} \approx 2.1$ Å, $k(\rho_{C1}) \approx 1 + 13.5\rho_{C1}$.

Let us consider first the ENDOR spectrum of $[(TPP)Fe(Im\text{-}d_4)_2]^+$ at g_{LF} (Figure 2a, trace 1). According to eq 14, at $g \approx 3$, the anisotropic hfi of the pyrrole protons is about −0.88 MHz. From the splittings of 1.08 (bb') and 1.68 MHz (aa') one then finds the isotropic hfi constants of about −0.2 and −0.8 MHz for two groups of pyrrole protons. A trial spectrum simulation with these hfi constants indicates that there are four protons in each group. The spin densities ρ_{C2} corresponding to these hfi constants obtained using eq 13 are about 0.003 and 0.013.

For the TPP complex, the ENDOR spectrum at g_{LF} is not sensitive to how the hfi constants are assigned to various pyrrole protons, because for all these protons $\mathbf{R_{FeH}}$ is at the same angle of 90° to $\mathbf{B_o}$. At g_{HF} ($g_{HF} = g_{11}$), on the other hand, $\mathbf{B_o}$ is in the heme plane and is at different angles to $\mathbf{R_{FeH}}$ for different protons. Therefore, the ENDOR spectrum at g_{HF} is not only sensitive to how the hfi constants are assigned to the particular protons, but also to the orientation of axis **1** in the heme plane (angle φ_1 in Figure 1).

The ENDOR spectrum at g_{HF} shown in Figure 2b (trace 1) is overwhelmingly dominated by the proton transitions at only one of the electron spin manifolds. To determine which manifold it is, we can consider the lines of the phenyl protons (marked by vertical dashed lines in Figure 6, whose two panels reproduce the ENDOR spectrum at g_{HF} as the top traces). The lower four traces in Figure 6, a and b, show the spectra of the phenyl protons simulated for the α and β electron spin manifolds, respectively, for various φ_1. Comparing the positions and relative intensities of lines in the experimental and simulated spectra, we find that the experimental ENDOR spectrum exhibits mainly the proton transitions corresponding to the β electron spin manifold, and $|\varphi_1| \in [25°...65°]$.

(41) Fessenden, R. W.; Schuler, R. H. *J. Chem. Phys.* **1963**, *39*, 2147.

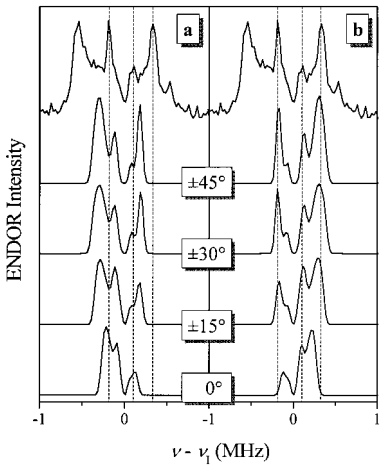

Figure 6. Top traces in both panels are the Mims ENDOR spectra of $[(TPP)Fe(Im\text{-}d_4)_2]^+$ at g_{LF} ($\mathbf{B_o} = 362$ mT) reproduced from Figure 2a. Other traces are simulations of the spectra of phenyl protons only, for different angles φ_1 (shown in the boxes along the line dividing the panels). In panel (a) only the nuclear transitions at α electron spin manifold, and in panel (b) only those at β electron spin manifold are shown. The vertical dashed lines indicate the position of prominent spectral features due to the phenyl protons.

Such an orientation of **1** is, most probably, caused by rotation of the imidazole ligand planes away from one of the N−Fe−N lines by the angle $\varphi_{lig} \neq 0°$.[42] From the ESEEM data presented below we find that for $[(TPP)Fe(Im\text{-}d_4)_2]^+$ $|\varphi_1 - \varphi_{lig}| \approx 55°$. Taken together with $|\varphi_1| \in [25°...65°]$, this yields the range of possible φ_{lig} from about 10° in the same direction to about 30° in the opposite direction.

To obtain guidance for assigning the large (−0.8 MHz) and small (−0.2 MHz) hfi constants of the protons at carbons $C_{(2)}$, the spin density distributions for various $\varphi_{lig} \in [-10°...30°]$ were estimated from Hückel molecular orbital calculations.[43] For every given φ_{lig}, φ_1 was chosen in such a way that $|\varphi_1 - \varphi_{lig}| \approx 55°$ and $|\varphi_1| \in [25°...65°]$. The simulations of the ENDOR spectra at g_{LF} and g_{HF} were then performed with variation of the hfi constants within narrow ranges around the values estimated above. As a result, we obtained nearly perfect simultaneous fits of the ENDOR spectra at g_{LF} and g_{HF} for $\varphi_1 \in [-35°...-30°]$ and $\varphi_{lig} \in [20°...25°]$ (see traces 2 in Figure 2, a and b, and the spin density distribution in Figure 7a). The resulting "best" hfi constants (2 × (−0.55 MHz), 2 × (−0.85 MHz), 2 × (−0.1 MHz) and 2 × (−0.2 MHz)) were split into two groups, large and small, with further small splittings within each group. These hfi constants are close to those assumed at the start of the calculation, and reflect the asymmetry in spin density distribution expected for $|\varphi_{lig}| > 0°$, but still significantly less than 45°.

The two subgroups of large hfi constants of −0.55 and −0.85 MHz are distributed over the protons at carbons $C_{(2)}$ of the pyrrole rings II and IV according to Figure 7a. The smaller hfi constants of −0.1 and −0.2 MHz are assigned to pyrrole rings I and III. Such an assignment originates from tracing the changes in the spin density distributions for different φ_{lig}. A minor disagreement with Figure 7a (where the larger spin densities in the rings I and III are close to the smaller spin densities in the rings II and IV) can be explained if we assume that $|\varphi_{lig}|$ is slightly smaller, and $|\varphi_1|$ is somewhat larger, than the values

(42) Shokhirev, N. V.; Walker, F. A. *J. Am. Chem. Soc.* **1998**, *120*, 981.

(43) MPORPH, an interactive simple Hückel program for DOS and Windows, with visualization of the orbitals, their nodal properties and energies is available: http://www.chem.arizona.edu/faculty/walk/nikolai/programs/html.

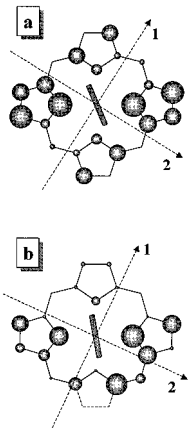

Figure 7. Spin density distributions estimated using Hückel molecular orbital calculations for $[(TPP)Fe(ImH)_2]^+$ (a) and $[(TPC)Fe(ImH)_2]^+$ (b). The rectangle at the center of each tetrapyrrole macrocycle represents the imidazole ligand. The values of φ_{lig} are 22.5° (a) and 10° (b). The orientations of the **g** tensor axes **1** and **2** found from our analysis of the ENDOR spectra ($\varphi_1 \cong -32°$ in (a) and $-25°$ in (b)) are also shown in these panels.

obtained in our calculations, which would indicate the limits of accuracy of our model for calculating the anisotropic hfi. Alternatively, the overlap integrals for the nitrogens N_I and N_{III} with Fe^{3+} in the Hückel calculations could be taken different from those for N_{II} and N_{IV}, which would reduce the spin densities in pyrrole rings I and III.

Apart from the small discrepancy mentioned, the overall spin density distribution obtained is in reasonable agreement with the qualitative results of the Hückel calculations shown in Figure 7a. The values of φ_1 and φ_{lig} obtained are in qualitative agreement with the principle of counterrotation that requires $\varphi_1 \approx -\varphi_{lig}$.[42] The above simulations show that our calculation model, despite its simplicity, is reasonably accurate and allows rather detailed conclusions to be made about the electronic structure of the iron porphyrinate complexes. Below, we will use a similar approach to the simulation of the ENDOR spectra of $[(TPC)Fe(Im\text{-}d_4)_2]^+$.

The ENDOR spectra of $[(TPC)Fe(Im\text{-}d_4)_2]^+$ at g_{LF} (trace 1 in Figure 3a) and g_{IF} (Figure 5) occupy the same frequency range as the spectra of the TPP complex, with the hyperfine splittings not exceeding 2.8 MHz. However, the spectra of $[(TPC)Fe(Im\text{-}d_4)_2]^+$ at g_{HF} (trace 1 in Figure 3b and traces 1−3 in Figure 4) show splittings of up to 4 MHz that correspond to the wings of very broad lines, the centers of which correspond to splittings of about 2.8 MHz. For brevity, we will refer to these lines simply as the "broad lines". Clearly, if the ground electronic state of the complex is $(d_{xy})^2(d_{xz},d_{yz})^3$, as is the case for $[(TPP)Fe(Im\text{-}d_4)_2]^+$, these lines cannot be attributed to the phenyl protons (see above).

In the low-spin iron(III) porphyrin complexes having the electronic state $(d_{xz},d_{yz})^4(d_{xy})^1$, an appreciable spin density was found at the heme *meso* positions and on the phenyl carbons.[38,44−46] In this case, from comparison of the NMR contact shifts of the pyrrole protons of $[(TPP)Fe(Im\text{-}d_4)_2]^+$ (about −20 ppm,[38] corresponding to $a_{iso} \leq -0.9$ MHz, see above) and of the phenyl protons in the $(d_{xz},d_{yz})^4(d_{xy})^1$ complexes (<13 ppm in absolute value[46]), the hfi constants of phenyl protons can be estimated as $|a_{iso}| < 0.6$ MHz. This value is far less than that required to explain the large splitting between the broad lines in our ENDOR spectra.

Therefore, the broad lines can only be assigned to the pyrrole or pyrroline protons. To limit the range of possible assumptions about these protons (α or β protons with positive or negative total hfi constant at g_{HF}) and the assignment of g_{HF} to g_{11} or g_{33}, calculations of the ENDOR splittings have been performed. In these calculations, based on eqs 13−16, the isotropic hfi constants for various angles θ_{1R} between **1** and $\mathbf{R_{FeH}}$ were calculated from the large ENDOR splitting at g_{HF}, and the splittings expected at g_{LF} and g_{IF} were then evaluated. An acceptable model should have predicted the splittings at g_{LF} and g_{IF} of no greater than the total width of the corresponding ENDOR spectra (≤2.8 MHz, which was checked by varying the time interval τ, see, e.g., Figure 5).

From these simulations we have found that the only model satisfying the experimental data is the one where the broad lines belong to the β protons pyrroline that have a positive total hfi constant at g_{HF}, $\theta_{1R} \leq 45°$, and g_{HF} corresponds to **1**. The ESEEM data (see below) show that g_{LF} corresponds to **3**. It thus follows that the electronic configuration of Fe^{3+} ion is $(d_{xy})^2(d_{xz},d_{yz})^3$, the same as that in $[(TPP)Fe(ImH)_2]^+$.

The broad outer features in the spectra at g_{LF} and g_{IF} (Figures 3a and 5) can also be with certainty assigned to the same protons (no such broad features were present in the spectra of the TPP complex). The more narrow lines located closer to the centers of all spectra are thus due to the protons of the phenyl and aromatic pyrrole rings.

The outer narrow features (aa') in the spectrum at g_{LF} (Figure 3a) have a splitting of about 1.1 MHz, from which $a_a \approx -0.35$ MHz can be estimated. The next pair of lines (bb') in the spectrum at g_{LF} has a splitting of about 0.7 MHz, which practically coincides with the dipole interaction of the pyrrole protons ($T_\perp \cong -0.74$ MHz at $R_{FeH} \cong 5.1$ Å). Two remaining pairs of lines with smaller splittings (cc' about 0.53 MHz and dd' about 0.2 MHz) should be assigned to the phenyl protons ($T_\perp \cong -0.59$ MHz, -0.21 MHz and -0.13 MHz for the *ortho*, *meta*, and *para* positions, respectively). From the trial simulation of the spectrum at g_{LF} it follows that there are only two pyrrole protons with $a_\alpha \approx -0.35$ MHz. The other four protons in the aromatic pyrrole rings have $a_\alpha \approx 0$ MHz.

We will now proceed with numerical simulations in order to refine the orientation of **1** in the chlorin plane and express it in terms of φ_1 rather than θ_{1R}. The range $|\theta_{1R}| < 45°$ for any of the β protons translates into $|\varphi_1| < 30°$. The simulations of the ENDOR spectra were performed for various φ_1 within this range. In these simulations, for a given φ_1, the isotropic hfi constants for the β protons were selected in such a way as to produce the pair of broad lines in the spectrum at g_{HF}. Because the exact shape of the broad lines is not precisely defined in the experiments, it was assumed that each β proton produced a pair of similar broad lines of Gaussian shape, with a splitting of 2.8 MHz, and the line width between maximum slope points of about 0.7 MHz. With these hfi constants, the spectra at g_{LF} and g_{IF} were then calculated. For acceptable angles φ_1, the positions of the H_b lines in the calculated spectra should have reproduced the positions of the broad outmost features in the experimental spectra at g_{LF} and g_{IF}.

The angle $|\varphi_1 - \varphi_{lig}| \approx 35°$ was estimated from the ESEEM measurements (see below). Therefore, for every trial φ_1, the spin density distributions were estimated using the Hückel

(44) Simonneaux, G.; HindrJ, F.; Le Plouzennec, M. *Inorg. Chem.* **1989**, *28*, 823.
(45) Walker, F. A.; Nasri, H.; Turowska-Tyrk, I.; Mohanrao, K.; Watson, C. T., Shokhirev, N., V.; Debrunner, P. G.; Scheidt, W. R. *J. Am. Chem. Soc.* **1996**, *118*, 12109.
(46) Simonneaux, G.; Schünemann, V.; Morice, C.; Carel, L.; Toupet, L.; Winkler, H.; Trautwein, A. X.; Walker, F. A. *J. Am. Chem. Soc.* **2000**, *122*, 4366.

method for $\varphi_{lig} = \varphi_1 \pm 35°$. These spin density distributions provided guidance for reasonable assignment of the isotropic hfi constants of the α- and β protons to particular positions in the aromatic pyrrole rings. The spectrum at g_1 calculated for such distributions of the hfi constants over the pyrrole protons should have reproduced, at least approximately, the positions and relative intensities of lines observed in the experimental spectrum.

As a result of these simulations, $\varphi_1 \cong -25°$ was found, with $\varphi_{lig} \cong 10°$. The spin density distribution corresponding to such a ligand orientation is shown in Figure 7b. The a_β values for the two pairs of β protons belonging to different $C_{(1)}$ were found to be about 1.6 and 2.15 MHz. Two protons in the aromatic pyrrole rings have $a_\alpha \cong -0.4$ MHz and are assigned to the positions in the pyrrole rings II and IV at the carbons $C_{(2)}$ having larger spin density (see Figure 7b). For all other protons in the aromatic pyrrole rings $a_\alpha = 0$ MHz was used. The ENDOR spectra at g_{LF} and g_{HF} simulated with these parameters are shown by traces 2 in Figure 3, a and b, respectively.

The quality of the simulations could be somewhat improved by varying the smaller hfi constants for the α protons within the range of ±0.1 MHz instead of keeping them at zero. This variation would, however, already exceed the accuracy of the model used herein for the anisotropic hfi. The intensity of the broad lines in the simulated spectrum at g_{HF} could be improved by considering these lines as consisting of two unresolved overlapped lines with different maxima. However, this results in cosmetic improvements only, and does not measurably change the estimate for φ_1 and overall spin density distribution in the π-system of $[(TPC)Fe(Im\text{-}d_4)_2]^+$.

Analysis of the ESEEM Results. The orientation of the imidazole ligand planes with respect to the **g** tensor axis **1** can be established by analyzing the position of the sum combination line of the imidazole protons 2 and 4 in the primary or four-pulse ESEEM spectra obtained at g_{HF}.[24] The details of the analysis and various experimental considerations have already been described[24] and will not be reiterated here. In these measurements, as in earlier measurements on similar systems,[21−23] the complexes with protonated imidazole ligands, Im-h_4, have been used. To increase the resolution of the sum combination line region in the ESEEM spectra, the measurements have been performed at S-band mw frequencies.

The transverse relaxation times of the TPP and TPC complexes were long enough ($T_2 \cong 3$ μs for both complexes) to provide sufficient resolution of the sum combination line region even in the primary ESEEM measurements. Figure 8 shows the primary ESEEM spectra of $[(TPP)Fe(Im\text{-}h_4)_2]^+$ and $[(TPC)Fe(Im\text{-}h_4)_2]^+$ corresponding to g_{HF}. We will not be interested in the low-frequency (<8 MHz) region of these spectra containing the lines of the distant solvent deuterons, nitrogen nuclei in the pyrrole and imidazole rings and by the proton fundamental line at the frequency of about 6 MHz. The frequency region of interest to us is in the vicinity of 12 MHz, where the proton sum combination lines are located. One can see that the sum combination feature in both experimental spectra consists of two lines. The one with the higher frequency (marked in Figure 8 "ν_σ close") is due to the imidazole protons 2 and 4 that are located at relatively short distance (3.1−3.3 Å) from the central Fe(III). The line with the lower frequency belongs to all the other, relatively distant protons, and is located almost exactly at the double Zeeman frequency of the protons, $2\nu_I$ (marked by a dashed line in Figure 8).

The upshift in frequency of the ν_σ line of the close protons (about 0.25 MHz for TPP and about 0.28 MHz for TPC) is proportional to the square of the nonsecular component of the anisotropic hfi, which, in its turn, depends on the angle $\Delta\varphi = |\varphi_1 - \varphi_{lig}|$ between the ligand planes and the **g** tensor axis **1**.[24] Simulating the primary ESEEM spectra for various trial values of $\Delta\varphi$ allows one to find the value of this angle for the systems under investigation.[24] With the aid of these calculations, assuming the ligand planes to be parallel, the angles $\Delta\varphi$ were found to be about 55° for the TPP complex and about 35° for the TPC complex. The spectra simulated for these ligand orientations are shown by the bottom traces in Figure 8, a and b. Since only protons were taken into account in our calculations, the simulated spectra do not contain lines due to other nuclei that crowd the low-frequency regions of the experimental spectra.

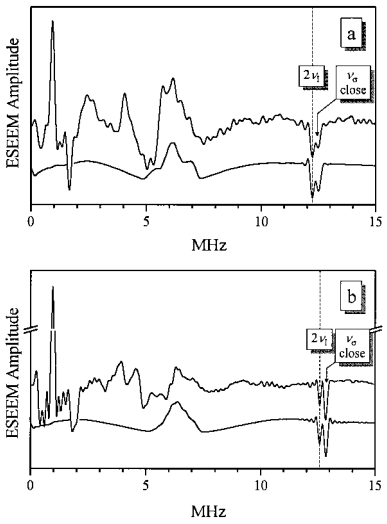

Figure 8. Top traces in panels (a) and (b) are the primary ESEEM spectra of $[(TPP)Fe(Im\text{-}h_4)_2]^+$ and $[(TPC)Fe(Im\text{-}h_4)_2]^+$, respectively, at g_{HF}. Experimental conditions: (a) $n_{mw} = 3.059$ GHz, $\mathbf{B_o} = 143$ mT; (a) $\nu_{mw} = 3.733$ GHz, $\mathbf{B_o} = 147.2$ mT. Bottom traces are the proton ESEEM spectra simulated for the imidazole ligand planes being parallel to each other, and at the angles of 55° (a) and 35° (b) with the axis **1** of the **g** tensor.

If the ligand planes are allowed to be at different angles to **1**, then the situation of the maximally nonparallel ligand planes can be described by the following angles $\Delta\varphi$: 40° for one ligand and 90° for the other ligand in the TPP complex, and 0° for one ligand and 65° for the other ligand in the TPC complex. Even for these large angles between the ligand planes, the angle between **1** and the bisector of the smaller angle between the ligand planes (which is actually essential for the Hückel molecular orbital calculations) is about 65° for $[(TPP)Fe(Im\text{-}h_4)_2]^+$ and 33° for $[(TPC)Fe(Im\text{-}h_4)_2]^+$, very close to the values obtained with the parallel planes.

There is good evidence based on the X-ray and single-crystal EPR studies, that for almost all complexes exhibiting **g** tensors similar to that of $[(TPP)Fe(Im\text{-}h_4)_2]^+$ the ligand planes are nearly parallel (the angle between the planes is less than 30°).[18,47−51] In fact, for single crystals of $[(TPP)Fe(Im\text{-}h_4)_2]^+$ itself, two types

(47) Little, R. G.; Dymock, K. R.; Ibers, J. A. *J. Am. Chem. Soc.* **1975**, *97*, 4532.
(48) Scheidt, W. R.; Osvath, S. R.; Lee, Y. J. *J. Am. Chem. Soc.* **1987**, *109*, 1958.
(49) Higgins, T.; Safo, M. K.; Scheidt, W. R. *Inorg. Chim. Acta* **1991**, *178*, 261.
(50) Hatano, K.; Safo, M. K.; Walker, F. A.; Scheidt, W. R. *Inorg. Chem.* **1991**, *30*, 1643.
(51) Munro, O. Q.; Serth-Guzzo, J. A.; Turowska-Tyrk, I.; Mohanrao, K.; Walker, F. A.; Debrunner, P. G.; Scheidt, W. R. *J. Am. Chem. Soc.* **1999**, *121*, 11144.

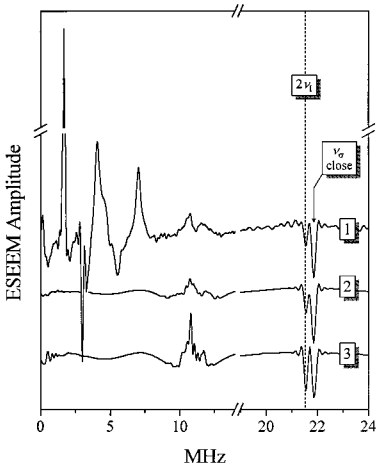

Figure 9. Primary ESEEM spectra of [(TPC)Fe(Im-h_4)$_2$]$^+$ at g_{LF} (ν_{mw} = 8.706 GHz, $\mathbf{B_o}$ = 252.4 mT). Trace 1, experimental. Trace 2, simulated assuming $g_{LF} = g_{33}$. Trace 3, simulated assuming $g_{LF} = g_{22}$. As in Figure 8b, the imidazole ligand planes were assumed to be parallel to each other and oriented at the angle of 35° with the **g** tensor axis **1**.

of molecules exist in the unit cell, both with the imidazole planes being parallel.[48] For the first type the plane orientation was close to the *meso* positions (41°) of the porphyrin ring, and for the second site the ligand planes were close to the N−Fe−N axis (6°). Since, as we have established from our ENDOR analysis, for the TPC complex the electronic ground state and the general arrangement of the **g** tensor axes are similar to those in [(TPP)-Fe(Im-d_4)$_2$]$^+$, we can expect that similar low-energy situations for the relative orientations of the ligand planes apply in this case too. Therefore, we conclude that the estimate of the angle between **1** and the bisector of the angle between the ligand planes is close to 55° and 35° for the TPP and TPC complexes, respectively. These are the angle values used in our calculations of the spin density distributions in these complexes.

To finish with the formal assignment of the EPR turning points to certain directions of $\mathbf{B_o}$ with respect to the molecular plane of [(TPC)Fe(Im-h_4)$_2$]$^+$, we may consider the possibility that g_{LF} corresponds to either **3** or **2**. To exclude one of these options, we will compare the experimental and calculated ESEEM spectra at g_{LF}. Trace 1 in Figure 9 shows the X-band primary ESEEM spectrum of [(TPC)Fe(Im-h_4)$_2$]$^+$ obtained at g_{LF}. Traces 2 and 3 are the spectra simulated assuming g_{LF} being associated with **3** or **2**, respectively. One can see that while spectrum 2 accurately reproduces the intensities of the sum combination features observed in the experimental spectrum, the intensity of the $2\nu_I$ line in spectrum 3 is considerably greater than the experimental one. It is not surprising that this line has a greater intensity at g_{22} since, for $\mathbf{B_o}$ being in the heme plane, the angles between $\mathbf{B_o}$ and the radius-vectors $\mathbf{R_{FeH}}$ for pyrrole protons in the aromatic rings generally differ from $n\pi/2$ (where n is an integer number). This results in noticeable nonsecular components of the anisotropic hfi that are responsible for the ESEEM intensity. Thus, the comparison of the experimental and simulated ESEEM spectra at g_{LF} allows one to conclude that g_{LF} is g_{33}, and thus g_{IF} is g_{22}.

Conclusions

In this work the ^{1}H pulsed ENDOR and multiband ESEEM spectra of the heme and imidazole protons of [(TPP)Fe(ImH)$_2$]$^+$ and [(TPC)Fe(ImH)$_2$]$^+$ at the canonical **g** tensor orientations were analyzed in detail to obtain the spin density distributions and the orientations of the **g** tensor axes in these systems. To perform the analysis, a computational strategy was developed with the following principal features: (1) the approximation for calculating the anisotropic hfi of the pyrrole protons took into account not only the contribution of the central Fe^{3+} ion but also the spin density on the carbon atoms participating in the heme π-system that are nearest to the protons of interest, (2) the qualitative results of Hückel molecular orbital calculations for various orientations of the imidazole ligand planes were used to provide guidance for assigning the larger and smaller spin densities to the pyrrole carbons, (3) the angle between the imidazole planes and the **g** tensor axis **1** was obtained from the ESEEM measurements and was used as a fixed parameter in the ENDOR simulations. This strategy has proved to be quite successful and can be applied for obtaining reliable information about the electronic structure of other ferriheme complexes, for which single-crystal EPR data are not available.

The most important conclusion of this work is that in [(TPC)-Fe(ImH)$_2$]$^+$, as in [(TPP)Fe(ImH)$_2$]$^+$, g_{LF} corresponds to g_{33}, and thus both complexes have the $(d_{xy})^2(d_{xz},d_{yz})^3$ electronic ground state in the molecular frame where axis **Z** is normal to the heme plane.

Acknowledgment. We are very grateful to Dr. Tatjana Kh. Shokhireva for synthesis of the (TPC)FeCl and preparation of the EPR samples with protonated and deuterated imidazole. In addition, we acknowledge the support of the National Science Foundation, Grants DIR-9016385 for purchase of the CW EPR spectrometer and BIR-9224431 and DBI-9604939 for construction of the two pulsed EPR spectrometers. F.A.W. acknowledges support of this research from NIH Grant DK-31038.

JA002777Y